Solid-State Phase Transition Induced by Pressure in $LiOH \cdot H_2O$

Elisa Di Pietro,[†] Marco Pagliai,[†] Gianni Cardini,*[,†,‡] and Vincenzo Schettino[†,‡]

Laboratorio di Spettroscopia Molecolare, Dipartimento di Chimica, Università di Firenze, Via della Lastruccia 3, 50019 Sesto Fiorentino, Firenze, Italia, and European Laboratory for Nonlinear Spectroscopy (LENS), via Nello Carrara 1, 50019 Sesto Fiorentino, Firenze, Italia

Received: March 15, 2006; In Final Form: May 10, 2006

When the free energy surface of the lithium hydroxide monohydrate crystal was explored, the high-pressure solid-state phase transition was determined. The high-pressure phase has been obtained through ab initio Car−Parrinello molecular dynamics simulation in the isothermic−isobaric ensemble. The recent metadynamics method has been applied to overcome the high activation energy barriers typical of rare events, like solid-state phase transition at high pressures. In the $LiOH \cdot H_2O$ system, there are two kinds of H bonds: water−water and hydroxyl−water. The effect of the pressure has been investigated, to give further insight into the high-pressure phase. The strengthening of the H bonds of the system produces modifications in the water and the hydroxyl ion dipole electronic environment. The infrared spectra of both phases have been calculated and compared with experiments, and the assignment of the external modes has been discussed.

1. Introduction

The structural and electronic properties of water molecules in crystals and in confined systems (like clathrates, zeolites, and ionic channels) are a topic of particular interest in both theoretical and experimental studies because of the ubiquitous presence of water in natural and biological systems.[1−4] In the present work, the properties of water molecules in the lithium hydroxide monohydrate crystal have been studied by ab initio molecular dynamics (MD) simulations.[5] $LiOH \cdot H_2O$ can be taken as an interesting model system, because it is know to exist in two different crystal phases,[6] one stable at ambient conditions (belonging to the monoclinic space group $C2/m$) and a second one, not completely characterized, stable at room temperature and at pressures above 33 kbar. Therefore, the electronic structures of water and the hydrogen-bond network can be studied in a system with a strong local electric field and an environment tunable with pressure through a structural phase transition.

In MD simulations of phase transitions, high energy barriers, much larger than the thermal factor, must be overcome, and this is hard to realize, because of the very limited duration of the simulation or because of size effects. Therefore, in MD simulations, crystal structures can be metastable far beyond their thermodynamic stability range. In several cases,[7−9] to overcome this problem, phase transitions have been forced to occur by an overpressurization of the sample. In the present work, the simulation of the $LiOH \cdot H_2O$ crystal phase transition from the ambient to the high pressure phase has been carried out in the framework of the recently proposed metadynamics (MTD) approach,[10,11] as implemented in the CPMD program.[5]

The MTD method, in the extended Lagrangian form, has been applied, coupled with classical dynamics[12,13] or tight-binding[12,14] and more recently with density functional theory,[15] with considerable success to structural transformations in condensed phases. In the present work, the MTD method has been used to allow for an efficient exploration of the free energy surface[11] in a feasible simulation time. By introducing in the Car−Parrinello[16]−Parrinello−Rahman[17] Lagrangian an appropriate memory-dependent potential, dependent on some selected collective variables, an initial basin of the free energy surface (corresponding to a starting structure) is progressively filled, avoiding a revisitation of the same phase space region until the system is captured in a new basin of attraction that hopefully corresponds to a different crystal phase. The MTD approach has been applied with success to $LiOH \cdot H_2O$ crystals; the phase transition has been observed, and both the ambient- and high-pressure phases have been fully characterized in particular as far as the electronic reorganization of the system is concerned. A detailed description of the hydrogen-bond network in the crystal in the two phases has been obtained by calculating the position of the electronic doublets by the centers of the maximally localized Wannier functions (MLWFC).[18,19] The electronic structure of the water molecules has been monitored by the molecular dipole moments. A comparison with available experiments of the high-pressure phase has been made by calculating the vibrational spectra.

2. Computational Details and Method

Ab initio Car−Parrinello[16] molecular dynamics simulations, using the CPMD code[5] that includes the MTD module, have been carried to obtain the phase transition of lithium hydroxide monohydrate at high pressures. To describe the electronic structure, the density functional theory[20] in the Kohn and Sham formulation[21] has been used. Norm-conserving pseudopotentials[22] have been adopted to calculate the interaction between the valence electrons and the frozen ionic cores. A Goedecker's pseupotential[23] for the Li atom, a Martins−Troullier's one[24] for the O atom, and a Car−von Barth's one[25] for the H atom have been adopted. The electronic wave functions have been expanded in plane waves with an energy cutoff at 70 Ry, allowing to a good approximation to the properties of the system. The exchange and correlation energy has been described by the

* Corresponding author tel.: 39-554573072; fax: 39-554573077; e-mail: gianni.cardini@unifi.it.
† Università di Firenze.
‡ European Laboratory for Nonlinear Spectroscopy.

10.1021/jp061620a CCC: $33.50
Published on Web 06/17/2006

Becke−Lee−Yang−Parr (BLYP) functional,[26,27] because this choice has been proved to give good results in similar systems, such as $Mg(OH)_2$,[28,29] $Ca(OH)_2$,[29] and LiOH.[15] The deuterium isotope has been adopted to allow for a larger time step.

To force the solid-state phase transition, the MTD method in the Iannuzzi−Laio−Parrinello (ILP) form[11] has been found effective. The total extended Lagrangian has the form

$$\mathscr{L} = \mathscr{L}^{\mathrm{CP-PR}} + \mathscr{L}^{\mathrm{ILP}} \tag{1}$$

where $\mathscr{L}^{\mathrm{CP-PR}}$ is the Car−Parrinello−Parrinello−Rahman Lagrangian:

$$\mathscr{L}^{\mathrm{CP-PR}} = \mu\sum_i \int |\dot{\psi}(\mathbf{s})|^2 + \frac{1}{2}\sum_I M_I(\dot{\mathbf{S}}_I{}^t\mathbf{h}^t\mathbf{h}\dot{\mathbf{S}}_I) - E[\{\bar{\psi}_i\}, \{\mathbf{h}\mathbf{S}_I\}] + \sum_{ij}\Lambda_{ij}(\int \psi_i{}^*(\mathbf{s})\,\psi_i(\mathbf{s})\,\mathrm{d}\mathbf{s} - \delta_{ij}) + \frac{1}{2}\mathbf{W}tr(\dot{\mathbf{h}}^t\dot{\mathbf{h}}) - p\Omega \tag{2}$$

In eq 2, μ is the fictitious mass of the electrons that has been chosen to equal 700 atomic units, $\{\psi_i\}$ are the Kohn−Sham orbitals, $\mathbf{S}_I$ are the ionic positions whose masses are indicated by M_I, $\mathbf{W}$ controls the inertia of the simulation cell and has been chosen to equal 30 000 atomic units, and Ω is the volume of the cell. The temperature has been set to 300 K. The symbol p refers to the hydrostatic external pressure. The estimate of the exact value of the internal pressure, at which the transformation occurs, is strongly affected by the Pulay forces.[30] Because the aim of this work is to determine the structural and dynamic properties of the high-pressure phase and to compare them with available experimental data,[6] no attempt has been made to exactly determine the transition pressure. Therefore, the calculations have been performed at an external pressure of 100 kbar.

The Iannuzzi−Laio−Parrinello Lagrangian, $\mathscr{L}^{\mathrm{ILP}}$, is

$$\mathscr{L}^{\mathrm{ILP}} = \sum_\alpha \frac{1}{2}M_\alpha\dot{s}_\alpha - \sum_\alpha \frac{1}{2}k_\alpha[S_\alpha(\{R_I\},\{\psi_n\},\{h_{ij}\}) - s_\alpha]^2 - V(t,\{s_a\}) \tag{3}$$

where $\{s_a\}$ is a set of coordinates, called collective variables (CV), which are functions of all degrees of freedom of the system. To obtain a meaningful description of the free energy surface and, therefore, of the phase transition, the CV must evolve with the system and be involved in the dynamic processes. The first and second terms in eq 3 couple the CV to the microscopic system via a harmonic potential. Through appropriate values of masses, M_α, and force constants, k_α, the dynamics of the CV, described by the first two terms of eq 3, can be decoupled from irrelevant fast motions.

For a solid-state phase transition, appropriated CV are the cell parameters defining the metric tensor $\mathbf{h}$.[12,15,31] In fact, their motion is slower if compared to other degrees of freedom of the system, and the dynamics of the CV is decoupled from the other motions. The same choice has been used with success in the study of the anhydrous LiOH high-pressure solid-state phase transition.[15]

Because we are only interested in the structural and electronic features of a new phase of $LiOH{\cdot}H_2O$ rather than the intermediate regions of the phase space, the Lagrangian of eq 3 can be simplified considering only the so-called time-dependent potential, $V(t,\{s_a\})$, expressed directly as a function of the metric tensor:

$$\mathscr{L} = \mathscr{L}^{\mathrm{CP-PR}} + V(t,\mathbf{h}) \tag{4}$$

TABLE 1: Cell Parameters of $LiOH{\cdot}H_2O$ at Room Conditions (phase I) and at High Pressure (phase II)[a]

	phase I exptl[38]	phase II calcd (this work)
a	7.4153 Å	5.24 Å
b	8.3054 Å	8.47 Å
c	3.1950 Å	3.67 Å
α	90°	107°
β	110.107°	94°
γ	90°	103°
vol	184.78 Å^3	148.99 Å^3
Z	4	4

[a] The high-pressure phase cell parameters refer to a conventional cell for a better comparison with phase I.

Equation 4 is equivalent to eq 1 in the limit of $k_\alpha \rightarrow \infty$ and $M_\alpha \rightarrow 0$. The contribution to the forces due to the time-dependent potential can be added directly to the stress tensor.

The time-dependent (or history-dependent) potential, $V(t,\{s_a\})$, is made of small, repulsive, Gaussian-like hills in the CV configuration space.[32]

Two kinds of simulations have been performed with an integration time step of 0.12 fs. To study the room-condition crystal structure, a simulation in the *NVE* ensemble has been carried on a sample with 48 atoms. The second kind of simulations has been performed to obtain the high-pressure phase and has been carried in the *NPT* ensemble on a super cell with 144 atoms, to reduce the effects of the approximation of limiting the wave functions expansion in plane waves to the Γ point adopted in Car−Parrinello molecular dynamics.

For the calculation of the IR spectra of phases I and II, two simulations in the *NVE* ensemble have been performed with an integration time step of 0.12 fs, storing at each time step for phase I and every eight time steps for phase II both the atomic configurations and the cell dipole moment, $M(t)$, computed in the Berry phase scheme[33−35] for a subsequent analysis. The infrared spectrum, $I(\omega)$, has been obtained by the Fourier transform of the autocorrelation function of $M(t)$:[36,37]

$$I(\omega) = \omega^2\int_{-\infty}^{+\infty} \mathrm{e}^{-i\omega t}\,\langle M(t)\,M(0)\rangle\,\mathrm{d}t \tag{5}$$

3. Phase Transition at High Pressure

The crystal structure of the lithium hydroxide monohydrate crystal at room temperature and pressure (phase I) has been obtained by neutron and X-ray scattering.[38] The conventional cell of $LiOH{\cdot}H_2O$ is monoclinic, belonging to the $C2/m$ space group, with the cell parameters reported in Table 1.

The structure of the ambient pressure phase is shown in Figure 1. It is made of rhomboidal units of water molecules and oxygens of OH^- ions about parallel to the *ab* plane. The rhomboidal units are linked by chains of OH^- ions along the *c* axis. The Li^+ ions are tetrahedrally coordinated to two hydroxyl ions and two oxygens of water molecules.

A first MD simulation, in the *NVE* ensemble, was carried starting from the ambient pressure structure to verify the reliability of our model. Salient geometrical parameters, obtained by minimization of the structure at 0 K, are reported in Table 2 along with the experimental data at 295 K[38] and the results of Hartree−Fock (HF) calculations with Gaussian basis sets[39] at 0 K; the latter are obtained by cell-parameter optimization. It can be seen that the results of the present simulation are in good agreement with experiments, and a considerable improvement with respect to HF calculations[39] has been obtained.

An initial MTD simulation in the *NPT* ensemble has been performed at ambient pressure. The evolutions of the volume

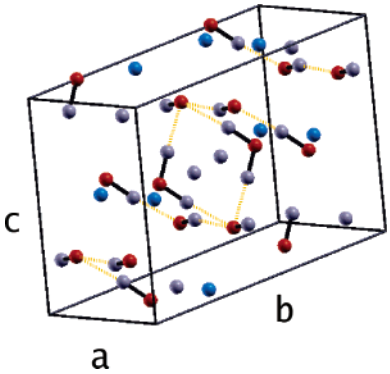

Figure 1. Conventional cell of $LiOH \cdot H_2O$ at room conditions (phase I). The Li^+ ions, the oxygen, and the hydrogen atoms are drawn in light blue, red, and gray, respectively, whereas the yellow dashed lines refer to H bonds. The cell parameters are $a = 7.4153$ Å, $b = 8.3054$ Å, $c = 3.1950$ Å, and $\beta = 110.107°$.

TABLE 2: Experimental and Calculated Intra and Intermolecular Distances (Å) and Angles (deg) Inside the Crystal

Structural Data				
		HF[39]		BLYP (this work)
distances (Å)[a]	exptl[38]	STO-3G	8-411g**	PW
O_w-H_w	1.002	1.018	0.967	1.019
O_h-H_h	0.951	0.987	0.947	0.969
$H_w\cdots O_h$	1.684	1.451	1.813	1.650
$H_h\cdots O_h$	2.259	2.052	2.300	2.259
$Li^+\cdots O_w$	1.982	1.757	2.032	1.970
$Li^+\cdots O_h$	1.965	1.768	1.946	1.987
angles (deg)[a]	exptl[38]	STO-3G	8-411g**	PW
$H_w-O_w-O_w$	104.3	100.7	106.0	104.3
$H_w-O_w\cdots O_h$	174.8	173.9	174.0	174.3
$O_h-H_h\cdots O_h$	167.6	173.7	169.3	167.5
$Li^+\cdots O_w\cdots L^+$	107.4	119.4	105.5	107.4
$O_h\cdots O_w\cdots O_h$	100.5	96.0	101.7	108.4
$Li^+\cdots O_h\cdots Li^+$	80.0	86.5	79.0	79.6

[a] With the subscripts h and w are labeled atoms of the hydroxyl and water groups, respectively.

and the energy are shown in Figure 2. After 2.6 ps (about 404 metadynamic steps, see Figure 2), several forward and backward transitions between phase I and an intermediate phase with some features, like a lower volume, of phase II have been observed.

An intermediate configuration (indicated by arrows in Figure 2) has been chosen as a starting point for a new MTD−*NPT* ensemble simulation increasing the pressure to 100 kbar. During this simulation, phase II appeared in a stable way after 3.2 ps (about 456 metadynamic steps, see Figure 3).

From the analysis of our data by the Platon suite of programs,[40] a $P\bar{1}$ cell symmetry was obtained for phase II, with the cell parameters reported in Table 1. The structure of the new phase is illustrated in Figure 4.

It is found that phase II is still centrosymmetric, in agreement with experimental data[6] that show that in the high-pressure phase the hydroxyl stretching mode has noncoincident infrared and Raman components. During the phase transition, a volume reduction of 19.4% has been found, essentially because of the contraction of the cell side *a* (see Table 1). In fact, when the rhomboidal units made by the oxygen atoms of two water molecules (O_w) and two hydroxyl ions (O_{ox}) are looked at, the O_w-O_w distance, approximately parallel to the *a* axis, decreases 8.3%. In phase I, the mean value of the O_w-O_w distance is 3.457 Å, and in phase II, it is 3.170 Å. On the other hand, the two $O_w-O_{ox}-O_w$ angles change from 81° to 76°.

4. Structural Properties

The radial pair distribution functions in the two phases are compared in Figure 5. It can be appreciated that the tetrahedral coordination of Li^+ to four oxygens present in phase I is maintained in phase II with a shortening of the Li···O distance from 1.99 to 1.89 Å. A shortening of the Li···H contacts is, likewise, observed in the high-pressure phase. The same occurs for the Li···Li contacts where, however, the shortening is particularly evident for the second shell with the second neighbor distance decreasing from 3.20 to 2.83 Å.

The most interesting information is obtained from the O···H pair distribution function. At shorter distances, two peaks are observed at 0.96 and 1.02 Å corresponding to the covalent bonds in H_2O and OH^- that are not much affected by pressure. The third peak appears at 1.68 and 1.56 Å in phases I and II, respectively. This gives an indication of the strengthening of the $O-H\cdots OH_2$ hydrogen bond in phase II. The hydrogen-bond strengthening is more pronounced for the O−H···O−H network, where the oxygen−hydrogen distance decreases from 2.26 to 1.91 Å. This feature is not evident from Figure 5E because of the broadness of the peaks. For this reason, we report in Figure 6 a specific O···H radial distribution function pertaining only to the contacts between hydroxyl ions. The salient data of the observed hydrogen bonds are summarized in Table 3. It can be seen from the angle values in the table that the O−H···O−H chains have a more pronounced zigzag arrangement in phase II. This finding is in agreement with the predictions of Adams and Haines[6] obtained from the analysis of the infrared spectrum.

It is evident that the significant changes observed in the cell parameters and in the radial distribution functions must be associated with a phase transition.

The electronic distribution in the two phases can be conveniently described by the MLWFCs. In phase I, as shown in Figure 7, the expected tetrahedral distribution of the MLWFCs around the oxygen atom of the water molecules has been found

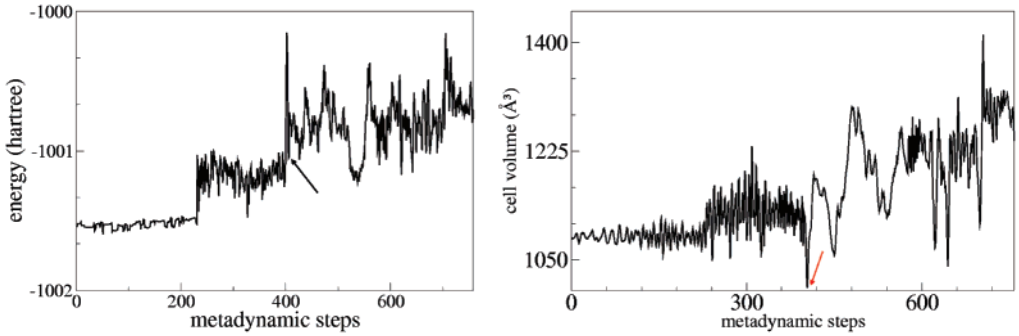

Figure 2. Fluctuation of energy and cell volume during the first metadynamics simulation. The arrows label a metastable configuration of phase II.

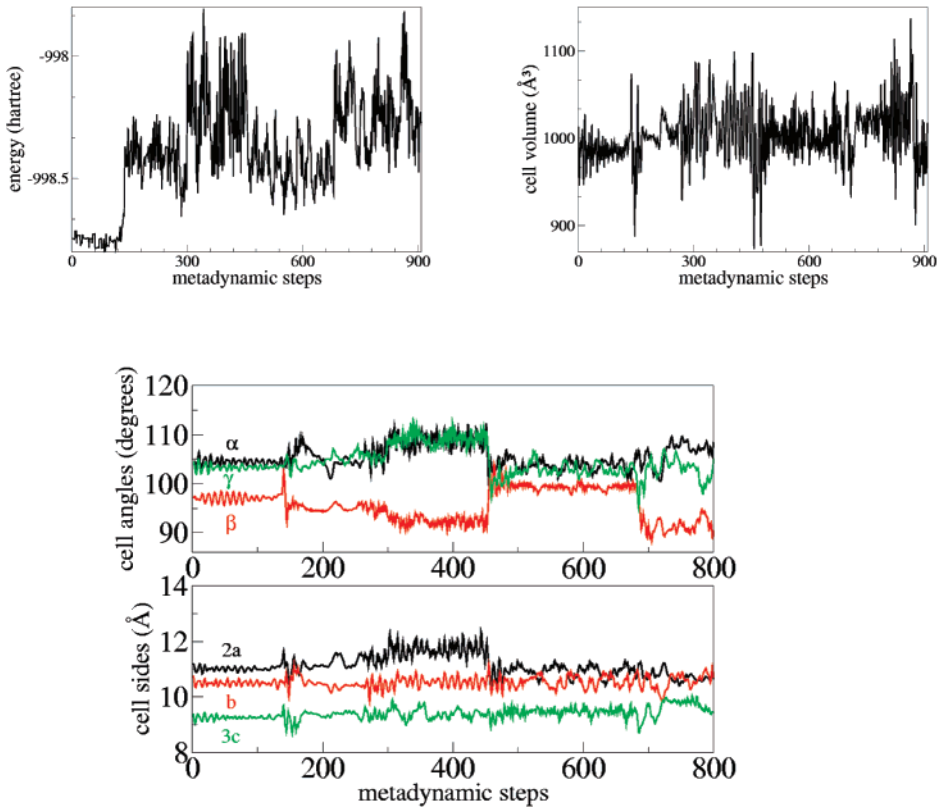

Figure 3. Fluctuation of energy, cell volume, and cell parameters during the second metadynamics simulation.

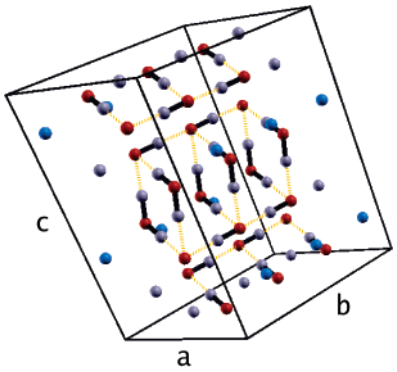

Figure 4. Conventional cell of $LiOH \cdot H_2O$ at high pressure (phase II). The Li^+ ions and the oxygen and hydrogen atoms are drawn in light blue, red, and gray, respectively, whereas the yellow dashed lines refer to H bonds. The cell parameters are $a = 5.24$ Å, $b = 8.47$ Å, $c = 3.67$ Å, $\alpha = 107°$, $\beta = 94°$, and $\gamma = 103°$.

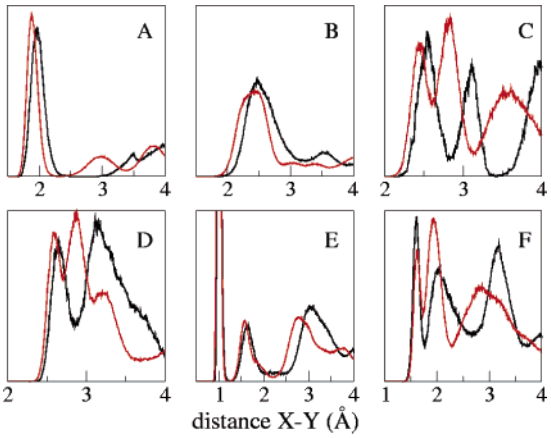

Figure 5. Radial distribution functions for all possible contacts in phase I (black lines) and phase II (red lines). **A**: Li···O contact. **B**: Li···H contact. **C**: Li···Li contact. **D**: O···O contact. **E**: O···H contact. **F**: H···H contact.

with two of the centers (corresponding to the lone pairs) pointing toward the two Li^+ ions. Among the four MLWFCs on the oxygen of the OH^- ion, two are oriented toward the hydrogen atoms of the H_2O molecules and one is placed along the Li−O−Li angle bisectrix.

Large electronic rearrangements occur upon phase transition, as it can be seen from Figure 8, where the changes of the MLWFC positions in the water molecule are shown. In Tables 4 and 5, the values of the distance from the oxygen atom of the MLWFCs in the hydroxyl ion and in the water molecule for both phases are reported, selecting the configuration at 0 K. In Table 4, the MLWFC positions show that in the high-pressure phase the H bonds of OH^- with water are not equivalent, because the w_2 and w_3 MLWFCs are at different distances from the O atom. Instead, in phase I, the MLWFC distances from the oxygen are equivalent.

The different strengths of the H bond in the two phases can also be deduced from the shorter O···H distance in phase II (see Table 3). The MLWFC position w4 is the shortest in both phases with a loss of symmetry of the free hydroxyl ion, because w4 is not involved in H bonds. In Table 5, the MLWFC positions around the O atom of the water molecule are reported. The C_2 molecular symmetry axis is conserved in both phases, with a slight lengthening of the MLWFC distance from the O atom in the high-pressure phase.

The changes of the electron distribution around the oxygen atoms of H_2O and OH^- in phase I of the $LiOH \cdot H_2O$ crystal compared to that of the isolate species have been discussed by several authors[38,39,41] on the basis of experimental X-ray diffraction data and ab initio calculations. It has been reported that in the crystal the electron distribution is driven away from the hydrogen toward the oxygen. This is confirmed by the data

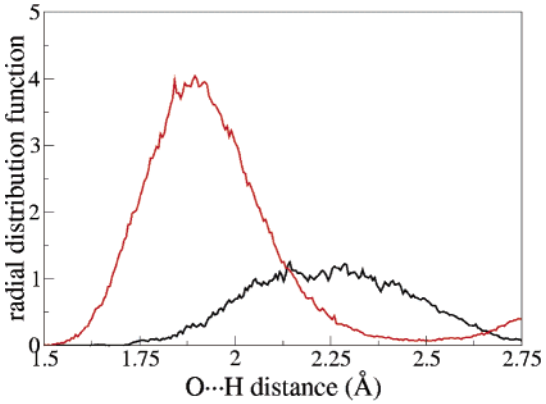

Figure 6. Plot of the O···H radial distribution function for phase I (black lines) and phase II (red lines) concerning the HO···HO contacts between hydroxyls.

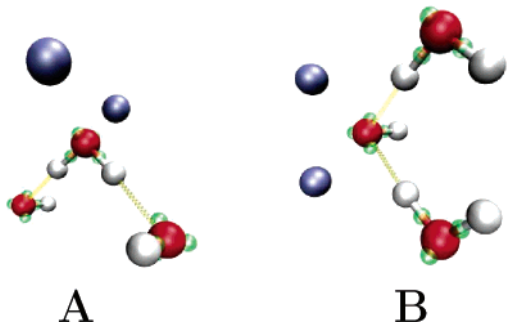

Figure 7. Distribution of electronic pairs around water molecules (A) and oxidryl ions (B). The MLWFCs, the Li^+ ions, and the oxygen and the hydrogen atoms are drawn in green, ice blue, red, and light gray, respectively, whereas the yellow dotted lines represent the H bonds.

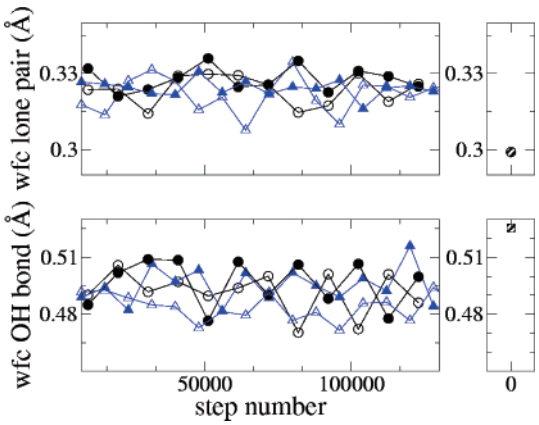

Figure 8. Distance between the MLWFC centers and the oxygen atom of a selected water molecule as a function of time at 300 K. In black and red, the phase I and phase II data are shown, respectively. In the right-hand panels, the MLWFC positions in the isolated molecule are shown.

TABLE 3: Summary of the Main Data on Hydrogen Bonds in the Two Phases of $LiOH·H_2O$

	phase I	phase II
r(OH···OH)	2.26 Å	1.91 Å
r(HOH···OH)	1.68 Å	1.56 Å
θ(OH···OH)	12°	17°
***θ*(HOH···OH)**	5.2°	5°

of Tables 4 and 5. Also, the finding[38,39,41] that the lone pair electron density around the oxygens decreases in the crystal is confirmed by the present calculations.

It is of considerable interest to analyze the thermal effects at room temperature. It has been found that quite large oscillations

TABLE 4: Distance from the Oxygen Atom of the MLWFCs in the Hydroxyl Ion in Both Phases for the Configuration at 0 K[a]

	OH^- free	phase I	phase II
w1 (Å)	0.569	0.5367	0.5131
w2 (Å)	0.326	0.3639	0.3669
w3 (Å)	0.326	0.3639	0.3655
w4 (Å)	0.326	0.3419	0.3478

[a] w1 is the MLWFC position in the intramolecular bond; w2 and w3 are the lone pairs pointing toward the hydrogens of water molecules, and w4 is the other lone pair around the oxygen atom. The same distances for the hydroxyl ion in a vacuum are reported in the first column.

TABLE 5: Distances from the Oxygen Atom of the MLWFCs in the Water Molecule in Both Phases for Configurations at 0 K[a]

	H_2O free	phase I	phase II
w5 (Å)	0.5263	0.4866	0.4881
w6 (Å)	0.5263	0.4880	0.4914
w7 (Å)	0.3008	0.3286	0.3323
w8 (Å)	0.3008	0.3304	0.3463

[a] w5 and w6 are the MLWFC positions between hydrogen and oxygen atoms; w7 and w8 are the MLWFC positions of the two lone pairs around the oxygen atom. In the first column, the same distances for the water molecule in a vacuum are reported.

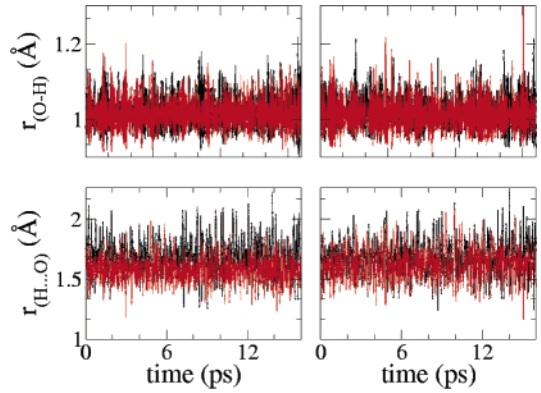

Figure 9. O-H bond length for a selected water molecule as a function of time. The black and red lines are related to phases I and II, respectively. In the upper panel are intramolecular bonds, and in the bottom panel are the intermolecular distances.

of the intra- and intermolecular O−H distances occur, as is shown in Figure 9 for a selected water molecule. In both phases the intramolecular O−H distance can stretch up to 1.2 Å, while the intermolecular distance shortens to reach a value as short as 1.3 Å. Even though these oscillations are quite large, there is no evidence from the present simulation, as there is no evidence from the infrared and Raman spectra, of the rapid exchange of protons between water and OH^- ions hypothesized by Tyutyunnik.[42]

The electronic rearrangement can be monitored by the dipole moments of the water molecules and the OH^- ions (see Figures 10 and 11). The average dipole moment of the water molecule is close to 3.60*D* in both phases, a value considerably larger than the 2.95*D*[43,44] obtained for liquid water using the same approach as that of the present work. This is likely a consequence of the strong local electric field in $LiOH·H_2O$. Hermansson and Lunell[41] hypothesized an increase of about 60% of the water molecule dipole moment in the lithium hydroxide monohydrate compared to the value in the free molecule. The present calculations predict a 40% increase of the dipole

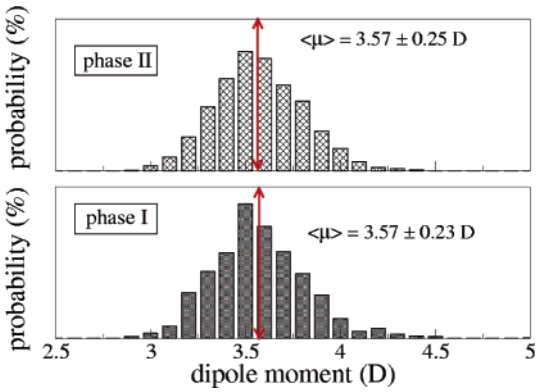

Figure 10. Dipole moment distribution of the water molecules in the $LiOH \cdot H_2O$ crystal.

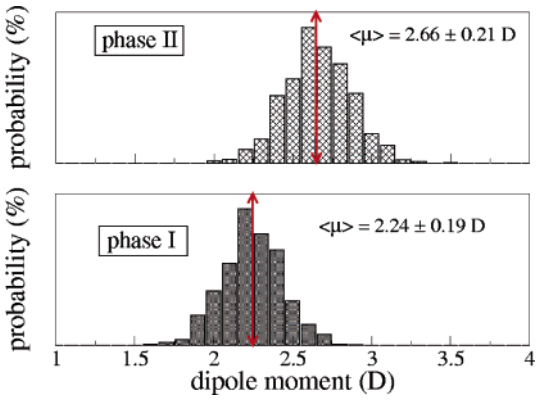

Figure 11. Dipole moment distribution of the hydroxyl ions in the $LiOH \cdot H_2O$ crystal.

moment, in qualitative agreement with Hermansson and Lunell's estimate.

The dipole moment has been calculated also for the OH^- ions, placing the origin of the vector on the oxygen atom. In this case, significant differences are found for the two phases, and the phase II average value is much larger as a consequence of the increased strength of the hydrogen bond and the larger extent of the charge transfer. This effect does not occur on the water molecule dipole moment, because the oxygen atom of the H_2O molecules is not directly involved in the hydrogen-bond strengthening in the high-pressure phase, and as a consequence, the associated charge transfer is small.

5. Spectroscopic Analysis

The vibrational spectra of phase I of $LiOH \cdot H_2O$ have been studied by several authors[42,45−47] and in particular by Hase,[46,47] who reported on the infrared and Raman spectra of several isotopic variants. The experimental spectra have been remeasured in the present work[48] and are in good agreement with previous reports except for the improved resolution of the infrared and Raman spectra and a few other details that will be discussed below. The spectrum of the high-pressure phase has been studied by Adams and Haines.[6,49] The assignment of the intramolecular modes is clear-cut, and we confine our discussion here to the external modes.

The bands assignment in phase I has been based mainly on isotopic shifts, in the assumption that there is a small coupling among different modes. However, the expected isotopic shifts for H_2O and OH^- rotational modes are not much different, while those of the translational modes are actually rather small. In the present work, the infrared spectrum of phase I has been calculated in the polarization parallel and perpendicular to the

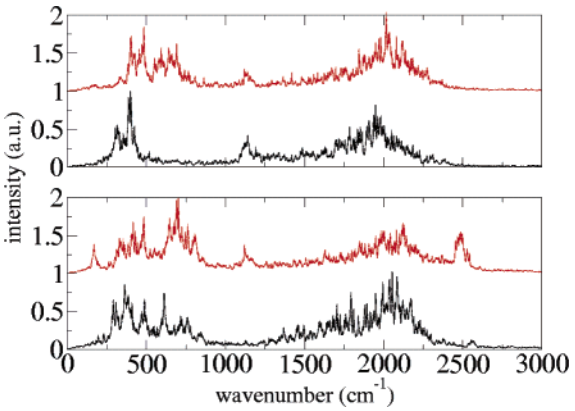

Figure 12. Calculated infrared spectrum of $LiOD \cdot D_2O$ in phase I (black line) and phase II (red line). In the upper panel, there is a spectrum with polarized light in the *y* axis, and in the bottom panel, there is a spectrum with polarized light in the *xz* plane.

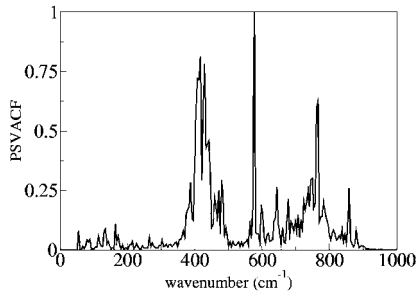

Figure 13. Power spectra of the velocity autocorrelation function of the lithium hydroxide monohydrate at room conditions in the 1−1000 cm^{-1} region.

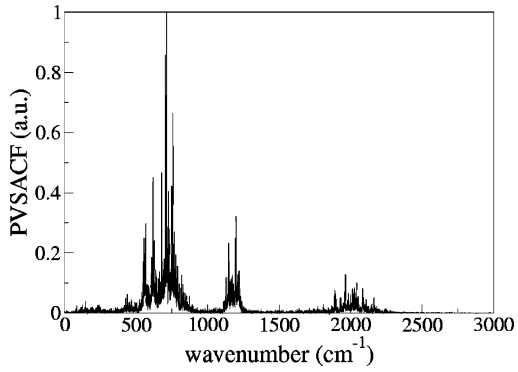

Figure 14. Power spectrum of the velocity autocorrelation function of the rotational modes of the D_2O molecules.

symmetry axis (see Figure 12). In addition, the power spectra of the velocity autocorrelational function (PSVACF), shown in Figure 13, have been calculated, and these data give the same indications as to the identification of the rotational modes, occurring in the most intricate region of the spectrum below 1000 cm^{-1}.

The total PSVACF shows in the 400−900 cm^{-1} a well-defined feature with five peaks. It is found that only the three high-frequency peaks are present in the PSVACF for the water molecules, while the other two appear in the power spectrum for the OH^- ions (see Figures 14 and 15). This is a clear indication for the bands assignment. In the *ac* polarized infrared spectrum, two peaks appear at higher frequencies that are associated with the water molecule rotations around the *x* (out-of-plane) and *y* (in-plane) molecular axes. The third water rotational mode (at the lower frequency of the triplet) is not observed in the calculated *b* polarized spectrum. This is not

TABLE 6: External Modes of Phase I of Lithium Hydroxide Monohydrate (cm^{-1})[a]

	$LiOH·H_2O$			$LiOD·D_2O$		
		exptl			exptl	
assignment	calcd[1]	IR	Raman	calcd	IR	Raman
$R_x(H_2O)$, $R_y(H_2O)$	974, 840	994(b_u), 855(b_u)	945(b_g)	700, 620	730(b_u), 632(b_u)	624(b_g)
$R_z(H_2O)$	792			560		
$R_1(OH^-)$	672	684(b_u)	700(a_g)	480	510(b_u)	468(a_g)
$R_2(OH^-)$	600	632(a_u)		430	468(a_u)	
$T(Li^+)$	420	494(a_u)	520(b_g)	400	485(a_u)	485(b_g)
$T(Li^+)$	410	456(b_u)	396(a_g)	390	450(b_u)	381(a_g)
$T(Li^+)$	378	413(b_u)	368(b_g)	360	398(b_u)	368(b_g)
		332	248	305/266	314	239
			214	215		206
translations			145	170		140
(H_2O and OH^-)			120	136		116
			95/80	90		93
			88	81		84

[a] The IR and Raman experimental frequencies lower than 450 cm^{-1} have been taken from Hase.[46,47]

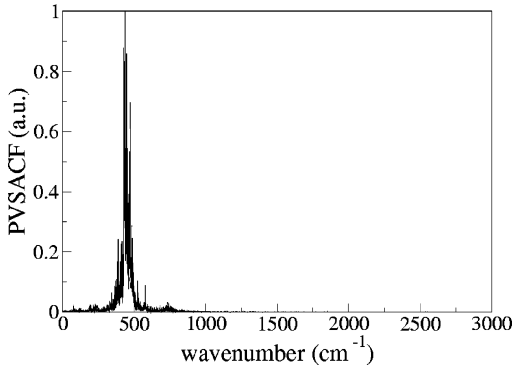

Figure 15. Power spectrum of the velocity autocorrelation function of the rotational modes of the OD^- ions.

surprising considering that in the oriented gas model approximation the rotation around the C_2 molecular axis will not develop an oscillating dipole moment. In the Raman spectrum only, a peak at 624 cm^{-1} is weakly observed. This can again be explained by the oriented gas model, considering that the polarizability tensor of the water molecule is almost spherical.[50] The OH^- rotational modes in $LiOD·D_2O$ are calculated at 430 and 480 cm^{-1} and correspond to the *b* (A_u) and *ac* (B_u) polarized modes.

When the theoretical isotopic ratios were used, the rotational mode frequencies of $LiOH·H_2O$ were obtained. The assignment is summarized in Table 6, and a very good agreement is found with experiments. We notice, however, that the Raman peak at 597 cm^{-1} reported by Hase[46,47] has not been observed in our spectra and has not been reported by Tyutyunnik[42] either. The occurrence of the H_2O librational modes at a higher frequency than that of the OH^- modes is in good agreement with the fact that in phase I the water molecules are involved in hydrogen bonds which contribute to larger force constants. However, it can be noted that the OH^- rotational modes occur at significantly higher frequencies than those in anhydrous lithium hydroxide,[51,52] implying that the crystal field in the hydrated compound is much stronger.

As to the translational modes, the related PSVACF clearly shows that the Li^+ modes are rather well decoupled from the H_2O and OH^- translations and occur in the region around 400 cm^{-1} (see Figure 16), in pretty good agreement with findings in the anhydrous compounds.[15]

A summary of the calculated frequencies and the assignment is contained in Table 6. While for the rotational modes the Raman and infrared corresponding components are close in frequency, the opposite is true for the Li^+ translational modes.

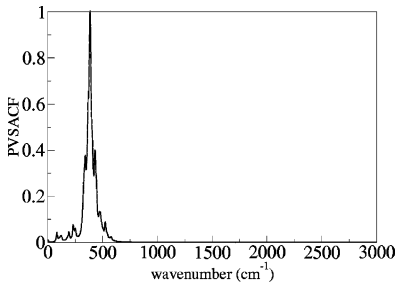

Figure 16. Translational modes of the Li^+ ion in the lithium hydroxide monohydrate at room conditions obtained through the PSVACF.

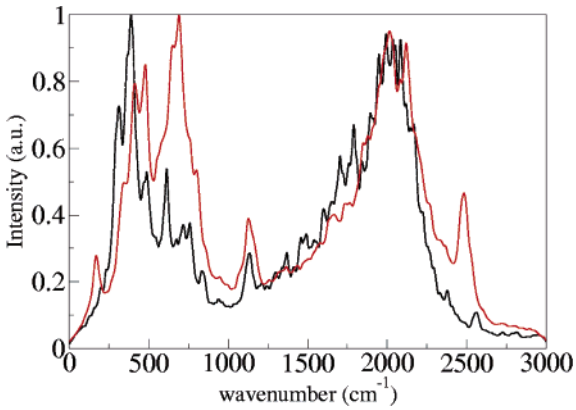

Figure 17. Comparison between the calculated infrared spectra of the room-condition phase (black line) and the high-pressure phase (red line).

The same has been found to occur for the Li^+ translational modes in anhydrous LiOH.[15]

In Figure 17, the calculated infrared spectra of the low- and high-pressure phases of $LiOD·D_2O$ are compared. The agreement with experiments is in general satisfactory. In particular, the OH^- stretching, that is, the most clear probe of the phase transition,[6] broadens and shifts to a lower frequency as a consequence of the involvement in hydrogen bonding, very much like it is observed experimentally.[6] In addition, in the high-pressure phase, the ν_{OH^-} peak has some structure that is reminiscent of the doubling observed experimentally.[6] In phase II, there is a red shift of the internal vibrational modes, while the external modes (rotational and translational) are in general blue-shifted. This is in overall agreement with experiments.[6]

6. Conclusions

The high-pressure phase of $LiOH·H_2O$ has been obtained with a new implementation of the metadynamics within the CPMD

method, and the environments of the water molecules and the OH^- ions in the two phases have been characterized.

The structure in the two phases has been analyzed by radial distribution functions, which allow an emphasis of the changes in the atomic environment with phase transition. By calculating the positions of the MLWFC, we have obtained a complete description of the rearrangement of the electronic pairs. The dipole moment distribution has been computed in both phases, and it has been observed that the average value of this quantity for the water molecule is closer to that found in ice rather than that in liquid water, but no substantial changes are associated with the phase transition. On the contrary, the dipole moment of the OH^- ion changes appreciably at the phase transition as a consequence of hydrogen-bond formation.

The agreement with experimental spectroscopic data for the high-pressure phase supports that metadynamics is a good tool to investigate the solid-state phase transitions.

Acknowledgment. We thank Dr. M. Iannuzzi for helpful discussions and Dr. M. Muniz-Miranda for the help in measuring the IR and Raman spectra. This work was supported by the Ministero dell'Istruzione, dell'Università e della Ricerca (MIUR).

References and Notes

(1) Gottardi, G.; Galli, E. *Natural Zeolites*; Springer-Verlag: Berlin, 1985.
(2) Crupi, V.; Majolino, D.; Venuti, V. *J. Phys.: Condens. Matter* **2004**, *16*, S5297.
(3) Klein, J.; Raviv, U.; Perkin, S.; Kampf, N.; Chai, L.; Giasson, S. *J. Phys.: Condens. Matter* **2004**, *16*, S5437.
(4) Demontis, P.; Suffritti, G. *J. Phys.: Condens. Matter* **2004**, *16*, 2845.
(5) Hutter, J.; Alavi, A.; Deutch, T.; Bernasconi, M.; Goedecker, S.; Marx, D.; Tuckerman, M.; Parrinello, M. *CPMD*; MPI für Festkörperforschung and IBM Zurich Research Laboratory: Stuttgart, Germany, 1995−1999.
(6) Adams, D. M.; Haines, J. *J. Phys.: Condens. Matter* **1991**, *3*, 9503−9509.
(7) Serra, S.; Chiarotti, G.; Scandolo, S.; Tosatti, E. *Phys. Rev. Lett*. **1998**, *80*, 5160.
(8) Scandolo, S.; Bernasconi, M.; Chiarotti, G.; Focher, P.; Tosatti, E. *Phys. Rev. Lett*. **1995**, *74*, 4015.
(9) Mizushima, K.; Yip, S.; Kaxiras, E. *Phys. Rev. B: Condens. Matter* **1994**, *50*, 14952.
(10) Laio, A.; Parrinello, M. *PNAS* **2002**, *99*, 12562.
(11) Iannuzzi, M.; Laio, A.; Parrinello, M. *Phys. Rev. Lett.* **2003**, *90*, 1.
(12) Martonák, R.; Laio, A.; Parrinello, M. *Phys. Rev. Lett*. **2003**, *90*, 075503.
(13) Raiteri, P.; Martonák, R.; Parrinello, M. *Angew. Chem., Int. Ed.* **2005**, *44*, 3796.
(14) Zipoli, F.; Bernasconi, M.; Martonák, R. *Eur. Phys. J. B* **2004**, *39*, 41−47.
(15) Pagliai, M.; Iannuzzi, M.; Cardini, G.; Parrinello, M.; Schettino, V. *Chem. Phys. Chem*. **2006**, *7*, 141.
(16) Car, R.; Parrinello, M. *Phys. Rev. Lett*. **1985**, *55*, 2471−2474.
(17) Parrinello, M.; Rahman, A. *Phys. Rev. Lett*. **1980**, *45*, 1196.
(18) Silvestrelli, P. L.; Marzari, N.; Vanderbilt, D.; Parrinello, M. *Solid State Commun.* **1998**, *107*, 7−11.
(19) Marzari, N.; Vanderbilt, D. *Phys. Rev. B: Condens. Matter* **1997**, *56*, 12847−12862.
(20) Hohenberg, P.; Kohn, W. *Phys. Rev.* **1964**, *136*, B864.
(21) Kohn, W.; Sham, L. *Phys. Rev.* **1965**, *140*, A1133.
(22) Kleinman, L.; Bylander, D. M. *Phys. Rev. Lett*. **1982**, *48*, 1425.
(23) Godeker, S.; Teter, M.; Hutter, J. *Phys. Rev. B: Condens. Matter* **1996**, *54* (3), 1703.
(24) Troullier, N.; Martins, J. L. *Phys. Rev. B: Condens. Matter* **1991**, *43*, 1993−2006.
(25) Vuilleumier, R.; Sprik, M. *J. Chem. Phys*. **2001**, *115*, 3454.
(26) Becke, A. D. *Phys. Rev. A: At., Mol., Opt. Phys.* **1988**, *38*, 3098−3100.
(27) Lee, C.; Yang, W.; Parr, R. G. *Phys. Rev. B: Condens. Matter* **1988**, *37*, 785−789.
(28) Churakov, S.; Iannuzzi, M.; Parrinello, M. *J. Phys. Chem. B* **2004**, *108*, 11567.
(29) Raugei, S.; Silvestrelli, P. L.; Parrinello, M. *Phys. Rev. Lett*. **1999**, *83*, 2222−2225.
(30) Dacosta, P.; Nielsen, O.; Kunc, K. *J. Phys. C: Solid State Phys.* **1986**, *19*, 3163.
(31) Martonák, R.; Laio, A.; Bernasconi, M.; Cerani, C.; Raiteri, P.; Zipoli, F.; Parrinello, M. *Z. Kristallogr*. **2005**, 220, 489.
(32) Details on the history-dependent potential parameters are available upon request to the authors.
(33) Tse, J. S. *Annu. Rev. Phys. Chem*. **2002**, *53*, 249−290.
(34) Resta, R. *Rev. Mod. Phys*. **1994**, *66*, 899−915.
(35) Vanderbilt, D.; King-Smith, R. D. *Phys. Rev. B: Condens. Matter* **1993**, *48*, 4442−4455.
(36) Guillot, B.; Marteau, P.; Obriot, J. *J. Chem. Phys*. **1990**, *93*, 6148−6164.
(37) Gaigeot, M.; Sprik, M. *J. Phys. Chem B* **2003**, *107*, 10344.
(38) Hermansson, K.; Thomas, J. O. *Acta Crystallogr., Sect. B* **1982**, *38*, 2555−2563.
(39) Ojamäe, L.; Hermansson, K.; Pisoni, C.; Causà, M.; Roetti, C. *Acta Crystallogr., Sect. B* **1994**, *50*, 268−279.
(40) Spek, A. *J. Appl. Crystallogr*. **2003**, *36*, 7.
(41) Hermansson, K.; Lunell, S. *Acta Crystallogr., Sect. B* **1982**, *38*, 2563−2569.
(42) Tyutyunnik, V. I. *J. Raman Spectrosc*. **2000**, *31*, 559−563.
(43) Silvestrelli, P. L.; Parrinello, M. *Phys. Rev. Lett.* **1999**, *82*, 3308−3311.
(44) Silvestrelli, P. L.; Parrinello, M. *J. Chem. Phys.* **1999**, *111*, 3572−3580.
(45) Gennick, I.; Harmon, K. M. *Inorg. Chem*. **1975**, *14*, 2214−2219.
(46) Hase, Y. *Inorg. Nucl. Chem. Lett.* **1980**, *16*, 159.
(47) Hase, Y. *Monatsce. Chem.* **1981**, *112*, 73.
(48) Raman spectra were obtained using the 514.5 nm line of an Ar^+ laser, a Jobin-Yvar HG25 monochromator equipped with a cooled RCA-C31034A photomultiplier, and a data aquisition facility. IR spectra were obtained by using a Perkin-Elmer FT-IR RX/I spectrometer. Solid samples were investigated in KBr pellets in the 4000−450 cm^{-1} spectral region. The commercial sample of lithium hydroxide monohydrate (99.995%) from Aldrich was used without further purification.
(49) Adams, D. M.; Haines, J. *J. Phys.: Condens. Matter* **1991**, *3*, 9503−9509.
(50) Cardini, G.; Schettino, V. *J. Raman Spectrosc*. **1984**, *15*, 237.
(51) Harbach, F.; Fischer, F. *J. Phys. Chem. Solids* **1975**, *36*, 601.
(52) Buchanan, R.; Caspers, H.; Marlin, H. *J. Chem. Phys.* **1964**, *40*, 1125.